Neuroinform (2014) 12:575–593
DOI 10.1007/s12021-014-9235-4

ORIGINAL ARTICLE

A Standardized [^{18}F]-FDG-PET Template for Spatial Normalization in Statistical Parametric Mapping of Dementia

Pasquale Anthony Della Rosa · Chiara Cerami · Francesca Gallivanone · Annapaola Prestia · Anna Caroli · Isabella Castiglioni · Maria Carla Gilardi · Giovanni Frisoni · Karl Friston · John Ashburner · Daniela Perani · and the EADC-PET Consortium*

Published online: 22 June 2014

Abstract [^{18}F]-fluorodeoxyglucose (FDG) Positron Emission Tomography (PET) is a widely used diagnostic tool that can detect and quantify pathophysiology, as assessed through changes in cerebral glucose metabolism. [^{18}F]-FDG PET scans can be analyzed using voxel-based statistical methods such as Statistical Parametric Mapping (SPM) that provide statistical maps of brain abnormalities in single patients. In order to perform SPM, a "spatial normalization" of an individual's PET scan is required to match a reference PET template. The PET template currently used for SPM normalization is based on [^{15}O]-H_2O images and does not resemble either the specific metabolic features of [^{18}F]-FDG brain scans or the specific morphological characteristics of individual brains affected by neurodegeneration. Thus, our aim was to create a new [^{18}F]-FDG PET aging and dementia-specific template for spatial normalization, based on images derived from both age-matched controls and patients. We hypothesized that this template would increase spatial normalization accuracy and thereby preserve crucial information for research and diagnostic purposes. We investigated the statistical sensitivity and registration accuracy of normalization procedures based on the standard and new template—at the single-subject and group level—independently for subjects with

*Alexander Drzezga and Robert Perneczky [Munich], Mira Didic and Eric Guedj [Marseilles], Bart N. Van Berckel and Rik Ossenkoppele [Amsterdam], Flavio Nobili and Silvia Morbelli [Genoa]

Electronic supplementary material The online version of this article (doi:10.1007/s12021-014-9235-4) contains supplementary material, which is available to authorized users.

P. A. Della Rosa (✉) · F. Gallivanone · I. Castiglioni · M. C. Gilardi
Institute of Molecular Bioimaging and Physiology, National Research Council, Segrate, MI, Italy
e-mail: pasquale.dellarosa@ibfm.cnr.it

C. Cerami · D. Perani (✉)
Vita-Salute San Raffaele University, Milan, Italy
e-mail: perani.daniela@hsr.it

C. Cerami
Clinical Neurosciences Department, San Raffaele Hospital, Division of Neuroscience, San Raffaele Scientific Institute, Milan, Italy

A. Prestia · G. Frisoni
IRCCS Centre San Giovanni di Dio - Fatebenefratelli, Laboratory of Epidemiology and Neuroimaging, Brescia, Italy

A. Caroli
Medical Imaging Unit, Bioengineering Department, IRCCS Mario Negri Institute for Pharmacological Research, Bergamo, Italy

M. C. Gilardi
University of Milan - Bicocca, Department of Health Sciences, Milan, Italy

G. Frisoni
Department of Psychiatry, Geneva University Hospital and University of Geneva, Geneva, Switzerland

K. Friston
Wellcome Trust Centre for Neuroimaging, Institute of Neurology, University College London, London, UK

J. Ashburner
Wellcome Trust Centre for Neuroimaging, London, UK

D. Perani
Nuclear Medicine Unit, San Raffaele Hospital, Division of Neuroscience, San Raffaele Scientific Institute, Milan, Italy

Mild Cognitive Impairment (MCI), probable Alzheimer's Disease (AD), Frontotemporal lobar degeneration (FTLD) and dementia with Lewy bodies (DLB). We found a significant statistical effect of the population-specific FDG template-based normalisation in key anatomical regions for each dementia subtype, suggesting that spatial normalization with the new template provides more accurate estimates of metabolic abnormalities for single-subject and group analysis, and therefore, a more effective diagnostic measure.

Keywords ^{18}F-FDG PET · SPM (RRID:nif-0000-00343) · Spatial normalization · Template · Dementia

Introduction

[^{18}F]-fluorodeoxyglucose-positron emission tomography ([^{18}F]-FDG PET) maps the distribution of glucose metabolism, which is driven mainly at the synaptic level (Magistretti 2000). Pathologic phenomena leading to neuritic dysfunction affect synaptic glucose consumption, before causing cell death and detectable atrophy. As such, [^{18}F]-FDG PET is a proxy for reduced glucose utilization by viable but potentially vulnerable neurones. [^{18}F]-FDG PET is thus a validated diagnostic tool, enabling the evaluation of brain function and dysfunction through regional changes in cerebral glucose metabolism (Sestini et al. 2010; Herholz et al. 2002; Anchisi et al. 2005; Salmon et al. 2009).

Twenty years of [^{18}F]-FDG PET imaging research have provided consistent patterns of hypometabolism/functional derangement, characterizing the different types of neurodegenerative diseases and significantly supporting clinical diagnosis (Teune et al. 2010; Teipel et al. 2013; Perani 2008). PET neuroimaging is gaining increasing importance in supporting differential diagnosis and it is now considered an essential part of the diagnostic protocol, helping to recognize typical patterns of dementia (McKeith et al. 2005; Dubois et al. 2010; McKhann et al. 2011; Sperling et al. 2011; Albert et al. 2011; Rascovsky et al. 2011). In Alzheimer's disease (AD), such a marker of functional neurodegeneration is considered to be more sensitive and to allow earlier diagnosis than conventional MRI (Jack et al. 2011).

At present, the clinical use of [^{18}F]-FDG PET imaging is mostly limited to the visual inspection of [^{18}F]-FDG uptake. This characterization is not optimal for a reliable diagnosis, especially for the earliest disease stages, when only subtle metabolic abnormalities may be present. It is also not ideal for localizing the topographical patterns that characterize different dementia conditions.

Approaches that overcome the subjective aspect of visual inspection include voxel-based analysis techniques, such as Statistical Parametrical Mapping (SPM) (Signorini et al. 1999), Neurostat (Minoshima et al. 1995) and t-sum (Herholz et al. 2002). These statistical parametric mapping procedures provide statistical maps of brain abnormality in single individuals, and are more accurate in detecting early changes and predicting subsequent conversion (Patterson et al. 2011; Berti et al. 2010; Chételat et al. 2003; Mosconi et al. 2008; Caroli et al. 2012).

The SPM package (SPM; Wellcome Trust Centre for Neuroimaging, London, U.K.), has been widely applied in [^{18}F]-FDG PET analysis for neurology research (Perani 2008). At the single-subject level, SPM provides the means for generating objective statistical maps, resulting from the comparison of one patient's scan to a group of control scans at the voxel level. To perform SPM, a "spatial normalization" of individual images is a mandatory prerequisite for statistical analysis. Spatial normalization is usually accomplished by spatially warping individual images to a template space, using an image registration algorithm. Spatial normalization requires a non-linear registration of PET images with a reference PET template, which is usually the standard [^{15}O]-H_2O template provided with the SPM software. After a geometric transformation, individual PET scans are transformed to a common neuroanatomical space, allowing voxelwise statistical analysis. When comparing a single [^{18}F]-FDG PET scan against a group of normal scans, it is important to minimize morphological differences between the patient and the normal scans, which could affect the metabolic comparisons producing statistical maps. Normalization indeed reduces morphological differences and anatomical variance in controls.

Depending on the PET radioligand, regional tracer uptake (i.e. the pattern of signal intensities in the [^{18}F]-FDG PET image) may not be represented properly by the pattern of signal intensities in the standard [^{15}O]-H_2O PET template (based on blood flow studies). A potential consequence of such a [^{15}O]-H_2O PET template normalization is that specific morphological features of an individual FDG brain cannot be matched to the template. This process introduces a potential loss of spatial normalisation accuracy—and in consequence, statistical efficiency—when comparing pathological scans against normal scans. This is especially so when studying neurodegenerative diseases, where morphological heterogeneity can be greatly increased by the underlying pathological process (Ishii et al. 2001).

Spatial normalization in SPM is based on minimizing the difference between an image and some template(s), subject to constraints on the plausibility of different deformations (Ashburner and Friston 1999). To find the optimal transformation, the image being normalized and the template(s) must have high mutual information that rests on the same spatial deployment of features (Ishii et al. 2001; Gispert et al. 2003). The choice of PET template image used for spatial normalization has been shown to influence statistical outcome (Gispert et al. 2003). Crucially, the use of [^{18}F]-FDG PET

and [^{15}O]-H_2O PET templates for normalizing [^{18}F]-FDG PET scans result in different spatial extents and peak heights of significant clusters in SPMs testing for metabolic changes (Ishii et al. 2001; Gispert et al. 2003).

The normalization bias—in the comparison between patients and controls—using voxelwise methods will tend to occur in atrophied brain regions. This normalization effect on statistical comparisons of metabolism, derived using the same spatial normalization for anatomically normal and atrophied brains, was investigated by Ishii et al. (2001), confirming that atrophied brains show artifacts introduced by the spatial normalization process. Crivello et al. (2002) also emphasized that spatial normalization can potentially confound quantification of inter-subject metabolic differences. Spatial normalization of pathological scans by matching them to a template derived only from a healthy control population will necessarily try to make pathological brains look normal. The spatial transformations will attempt to reduce any mismatch between image and template—and potentially confound anatomical and metabolic differences. A strategy to overcome this confound would be to use the scans of patients to compute a pathology-specific template that is representative of the population under investigation. This procedure should minimize conflation of anatomical and metabolic differences in the way that has been established in structural MRI procedures such as Voxel Based Morphometry (VBM) (Good et al. 2001) or through registration schemes that create population-specific templates, such as DARTEL (Ashburner 2007).

In most [^{18}F]-FDG PET studies, however, the use of the standard [^{15}O]-H_2O PET template still remains the most common choice for spatial normalization. Regarding [^{18}F]-FDG PET, the possible differences in statistical maps of brain metabolism ascribed to the use of different templates has not been investigated in depth (Ishii et al. 2001; Gispert et al. 2003), and—so far—has been ignored in the context of the analysis of single patients with suspected dementia. SPM is not intended for the detection of metabolic dysfunction with a particular tracer, in a particular neurological condition (i.e., dementia) at the single-subject level and does not come prepackaged with an [^{18}F]-FDG PET population-specific template. SPM spatial normalization for statistical analyses of [^{18}F]-FDG PET images may thus benefit from the availability of a dedicated template and the validation of the accuracy of the ensuing spatial normalization, particularly for pathological [^{18}F]-FDG PET images.

In summary, our aim was to create a new [^{18}F]-FDG PET population-specific template for spatial normalization, based on images derived from both patients (sample of scans representative of the various forms of dementia in the population) and age-matched controls. Our strategy for constructing a reference template for this particular application eschews any assumptions about the mapping between structural and metabolic anatomy that underlies the use of MRI-based registration. In other words, the functional anatomy defined operationally by regional glucose metabolism is used directly to provide an average template. This ensures that the spatial scale of metabolic anatomy that is conserved over subjects is retained in the template—and is not confounded by matching the detailed anatomy in high resolution structural images. Our hypothesis was that spatial normalization with these templates would provide a higher degree of registration accuracy and minimize the conflation of anatomical and metabolic differences between patients and control subjects. To this end, we report a study that comprised the following steps:

1) Creation of an [^{18}F]-FDG PET dementia-specific template (Gispert et al. 2003; Wenzel et al. 2010)
2) Implementation of a [^{15}O]-H_2O-specific and a [^{18}F]-FDG-specific spatial normalization of both patient and normal [^{18}F]-FDG PET scans into standard MNI stereotactic space
3) Empirical validation—in terms of cluster extent, anatomical validity and statistical efficiency—of each normalization procedure (i.e., [^{15}O]-H_2O and [^{18}F]-FDG) in single-patient vs. normal group analysis and in groups of patients affected by different forms of dementia.

Materials & Methods

[^{18}F]-FDG PET Template Creation

Healthy Control and Patient Images for the [^{18}F]-FDG PET Template Creation

To create an [^{18}F]-FDG PET template—representative of the specific features of FDG brain scans for neurodegenerative purpose—we collected a total of 120 [^{18}F]-FDG PET images from 60 healthy subjects (HC) (23 men and 32 women; mean age=69.80 years; standard deviation (SD=7.49 years) and from 60 patients with dementia (23 men and 32 women; mean age=72.65 years; SD=9.08 years), matched pair-wise for age and sex (Pair-wise Mean Difference between Controls and Patients (Δ AGE=2.85; p=0.07).

The 60 HC represented a subset of two large databases of [^{18}F]-FDG PET brain images (see below), collected under the auspices of the European Alzheimer's Disease Consortium (EADC) group (N=113) and of San Raffaele Scientific Research Institute (uHSR) (N=19) (see Table 1).

The 60 patients were sampled according to the incidence of degenerative cognitive decline in western countries (e.g. Prince et al. 2011; Bornebroek and Bretelera 2004), we selected 36 patients who fulfilled clinical consensus criteria for probable AD (Dubois et al. 2010; McKhann et al. 2011) (60 %

Table 1 Number of selected healthy controls in each centre and characteristics of PET scanners and image acquisition used to create the [^{18}F]-FDG PET template

Centre	Number of scans	Scanner manufacturer	Scanner type	Spatial resolution		Axial field of view (mm)
				In-plane FWHM	Slice thickness	
uHSR, Milan	19 HC	GE Healthcare, UK	Discovery STE	5.55	3.27	154
EADC (centre)						
Brescia	27 HC	GE Healthcare, UK	Discovery ST	5.99	2.34	157
Amsterdam	21 HC	Siemens, Germany	ECAT EXACT HR+	7.00	2.50	155
Genoa	36 HC	Siemens, Germany	Biograph Hi-rez	5.80	3.75	162
Munich	19 HC	Siemens, Germany	ECAT EXACT HR+	7.00	2.46	155
Marseille	10 HC	GE Healthcare, UK	Discovery ST	6.20	3.27	157

uHSR San Raffaele Scientific Research Institute, *EADC* European Alzheimer Disease Consortium, *FWHM* Full Width at Half Maximum, *HC* healthy controls

of the overall sample), 12 patients affected by Mild Cognitive Impairment (MCI) (Winblad et al. 2004), including those fulfilling criteria for prodromal AD (Sperling et al. 2011; Albert et al. 2011), 6 behavioral variant of Frontotemporal Dementia (bvFTD) (Rascovsky et al. 2011; Neary et al. 1998; McKhann et al. 2001), and 6 patients affected by Dementia with Lewy bodies (DLB) (McKeith et al. 2005).

All healthy subjects and patients provided written consent prior to their inclusion in the study, which was carried out in accordance with the Code of Ethics of the World Medical Association (Declaration of Helsinki) for experiments involving humans.

An [^{18}F]-FDG PET brain study was performed in all subjects (healthy controls and patients) according to conventional neurological acquisition protocols and to the European Association of Nuclear Medicine (EANM) guidelines (Bartenstein et al. 2002; Morbelli et al. 2012).

Before radiopharmaceutical injection, subjects were fasted for at least six hours to ensure measured blood glucose level was <120 mg/dL. Subjects underwent a 3D PET scan (time interval between injection and scan start ranged from 30 to 45 min; scan duration ranged from 10 to 15 min depending on the PET scanner characteristics) after the injection of [^{18}F]-FDG (185–250 Mbq: usually, 5–8 mCi via a venous cannula). Images were reconstructed using an ordered subset expectation maximization algorithm in all centers but Amsterdam (which used filtered back projection). Attenuation correction was based on CT scans in Milan, Brescia, Genoa, and Marseille, and on transmission scans in Munich and Amsterdam. Specific software integrated in each scanner was used for scatter correction. The scanner technical details and image acquisition characteristics for scanner type and subject group are reported in Table 1.

Spatial Normalization of [^{18}F]-FDG PET Images

The 120 [^{18}F]-FDG PET images (60 HC and 60 patients) were scaled to the same maximum and minimum range, in order to minimize differences in the image scaling factors due to different scanners.

The 120 [^{18}F]-FDG PET scaled images were then spatially normalized to MNI space. Following manual rotations and translations in order to grossly align each [^{18}F]-FDG PET image to MNI space, a customized automatic reorientation procedure was applied to match each [^{18}F]-FDG PET image to the [^{15}O]-H_2O PET template provided with SPM, enabling a more accurate spatial normalization process. All image-processing from this point on was performed using SPM5 under (www.fil.ion.ucl.ac.uk/spm), running in Matlab 7.6 (MathWorks Inc., Sherborn, MA). To place the 120 [^{18}F]-FDG PET images in the standard MNI space, the MNI-based [^{15}O]-H_2O PET template provided with SPM5 was used, following the strategy described in Signorini et al. (1999) and according to the procedure for functional normalization described in Gispert et al. (2003). In particular, to spatially normalize [^{18}F]-FDG PET images with this template, we used the normalization algorithm provided by SPM5, that employs a 12-parameter affine transformation followed by nonlinear deformations. Basis functions for the nonlinear warping were 7×8×7 in x-, y-, and z-dimensions, respectively, with 16 iterations. The following SPM5 default parameter settings were used for estimating the spatial transformations: no template and source weighting; 25 mm cutoff; medium regularization; 16 nonlinear iterations. The "Preserve Concentration" setting, along with trilinear interpolation, was used to create the normalized images. The field of view (FOV) used for the spatially normalized images was set to that of the other templates released with SPM5, with an isotropic voxel size of 2 mm.

Each normalized [^{18}F]-FDG PET image was visually inspected to assess the spatial normalization quality and to ensure the spatial normalization converged to an appropriate solution.

Intensity Normalization of [^{18}F]-FDG PET Images

The final set of normalized images were first "count normalized" (Yakushev et al. 2009) in order to standardize the magnitude of all voxel values in every image using the count scaling algorithm implemented as default by SPM (Friston et al. 1994; Buchert et al. 2005) and then rescaled to have the same mean intensities prior to averaging, so that all images would contribute equally to the template: this accounts for center-specific image scaling as well as for variability in the amount of injected radioactivity. Furthermore, it ensures that the intensity of each image (normal or pathological) contributes in a balanced way to the average image (template). Distance analysis (Kherif et al. 2003) was used to perform outlier diagnosis, with respect to inter-subject variation and noise from outside the brain. First, the SPM masking toolbox (Ridgway et al. 2009) was used 1) to compute a mean image from the spatially and intensity normalized [^{18}F]-FDG PET images and 2) to create a template-specific explicit optimal threshold within-brain mask. The within-brain mask was used to eliminate variance due to inter-subject variation and noise from outside the brain. We first inspected a matrix of distances between all pairs of images, which indicated how far any given scan was from each another, thus revealing outlier scans.

We then tested for the influence of a particular scan on the average (Cook test). This averaging procedure can be regarded as a form of robust averaging that suppresses outliers.

"Soft Mean" and Smoothing of [^{18}F]-FDG PET Images

The final spatially and intensity normalized [^{18}F]-FDG PET images were averaged using a "soft mean", to obtain a mean [^{18}F]-FDG PET image that conforms to the standard stereotaxic space defined by the MNI/International Consortium for Brain Mapping (ICBM) 152 MNI templates, as supplied with SPM. Depending on the field of view, this soft-mean results in a slightly different variance at voxels where different numbers of images have contributed, meaning that—at each voxel—the mean was computed via a floating-point relative accuracy function over only those images that have a value in that location.

The resulting "[^{18}F]-FDG-PET" template was smoothed with an isotropic 3D Gaussian kernel of 8 mm FWHM to reduce high spatial frequency noise and match the spatial resolution of the H_2O-PET template provided with SPM.

Validation of the [^{18}F]-FDG PET Template

We validated the new [^{18}F]-FDG PET template by evaluating the impact of its clinical use in a SPM analysis of single-subject [^{18}F]-FDG PET studies of patients versus healthy controls. Single-subject [^{18}F]-FDG PET study is the current standard SPM design for clinical purposes, since clinicians need to perform diagnosis on a single subject level in their clinical routine (Signorini et al. 1999).

Our validation was focused on the effect of using the [^{18}F]-FDG PET template with respect to the [^{15}O]-H_2O PET template for:

1) assessment of "normality rate",
2) single patient SPM analysis versus healthy controls at four levels:

   a) hypometabolism SPM-t approach,
   b) hypometabolism ROI approach
   c) hypometabolism second level analysis for whole-brain pattern approach
   d) diagnostic effectiveness.

Database of [^{18}F]-FDG PET Healthy Control and Patient Images for the Clinical Validation

A group of healthy control [^{18}F]-FDG PET scans was selected from the EADC and uHSR centers' databases. [^{18}F]-FDG PET images were acquired among different centers according to conventional neurological acquisition protocols and to the European Association of Nuclear Medicine (EANM) guidelines (Bartenstein et al. 2002; Morbelli et al. 2012) under the same conditions and using the same scanning protocol used for normal and patient scans selected for the creation of the [^{18}F]-FDG PET template.

Controls had a negative history for neuropsychiatric and neurological disorders or chronic illness. Balancing for the impact of different scanner among centers, with the only criteria to cover the age range of the demented population, a total of 132 scans of HC (62 men and 70 women; mean age=65.19 years; SD=9.21 years; age range=40–83 years) was used: uHSR database (19 subjects), EADC database: Brescia (27 subjects), Genoa (36 subjects), Munich (19 subjects), Amsterdam (21 subjects), Marseille (10 subjects) (see Table 1 for details).

We selected a large sample of [^{18}F]-FDG PET scans (n=67) pooled from the dementia population acquired at the uHSR center in Milan, in order to compare single-subject-versus healthy control group statistical effects in specific brain regions. Namely, we selected 23 cases diagnosed with AD (Dubois et al. 2010; McKhann et al. 2011) or prodromal AD (i.e., MCI patients with positive biomarkers of AD) (Sperling

et al. 2010; Albert et al. 2011); 24 cases fulfilling current clinical criteria for bvFTD (Rascovsky et al. 2011; Neary et al. 1998; McKhann et al. 2001) and 20 DLB patients (McKeith et al. 2005).

Spatial Normalization of [^{18}F]-FDG PET Images

[^{18}F]-FDG PET images from both healthy controls and patients were normalized using SPM5 (www.fil.ion.ucl.ac.uk/spm), running in Matlab 7.6 (MathWorks Inc., Sherborn, MA). We first performed approximate manual image reorientation and positioning to MNI space. Specifically, [^{18}F]-FDG PET images of healthy controls and patients were normalized and smoothed following each of the two normalization procedures described hereafter: normalization to the [^{15}O]-H_2O PET template and normalization to the [^{18}F]-FDG PET template.

The [^{15}O]-H_2O PET template provided with SPM5 was built by averaging and smoothing (with an 8-mm FWHM Gaussian filter) 12 Oxygen-15-labeled water PET scans (www.fil.ion.ucl.ac.uk/spm/spm99.html). This template is the most commonly used to spatially transform PET images to the MNI (Montreal Neurological Institute) reference space (Evans et al. 1993), regardless of the tracer employed.

To spatially normalize the [^{18}F]-FDG PET images to this template, we used the normalization algorithm provided by SPM5 with the following parameter settings including 12-parameters' affine transformation, 7×8×7 discrete cosine transform basis functions, no template and source weighting; discrete cosine transform cutoff: 25 mm; 16 nonlinear iterations and the nonlinear regularization term set to 1. No modulation ("preserve concentrations") and trilinear interpolation was used during final re-slicing. The dimensions of normalized images were x=−78:78; y=−112:76; z=−50:85 mm from the anterior commissure with 2×2×2 mm^3 isotropic voxels.

A visual inspection of all normalized images was performed with the exclusion of images with partial FOVs or where the normalization procedure failed, with the purpose to confirm spatial normalization convergence.

The "[^{15}O]-H_2O" normalized scans underwent further processing steps in order to minimize possible differences induced by the specific imaging characteristics and scanning protocols of each PET center. A two-pass masked-normalization was applied with the purpose of include in the statistical analysis only those signal voxels included in the mask. In the first pass a scanner-specific mask was applied in order to exclude voxels not included in all the images from the same scanner. In the second pass a conjoint mask was created as a binary image including only voxels covered by each image from each considered scanner.

Furthermore, the "[^{15}O]-H_2O" normalized scans from healthy control database underwent an intensity rescaling and a global count intensity normalization to have the same mean intensities (Friston et al. 1994; Buchert et al. 2005) and a subsequent distance analysis to exclude outliers.

The PET images for both normal subjects and patients were spatially normalized to the [^{18}F]-FDG PET Template under the identical pipeline implemented for [^{15}O]-H_2O PET template spatial normalization, with the algorithm provided by SPM5 using the same settings. The "[^{18}F]-FDG" functionally normalized PET scans from healthy controls were submitted to the same post-processing steps and quality control described for the "[^{15}O]-H_2O" normalized scans.

The two spatially normalized images resulting from each independent normalization procedure were then smoothed with a 3D Gaussian kernel of 8 mm FWHM, and entered into a single subject vs. healthy control group statistical analysis.

Assessment of "Normality" Rate

To test how the [^{18}F]-FDG PET template performs in assessing "normality" with respect to the standard [^{15}O]-H_2O procedure, we calculated false positive rates (percent of misclassified individuals) obtained during a leave-one-out approach.

Both reference databases of normalized healthy controls (i.e., healthy control [^{18}F]-FDG PET images spatially and intensity normalized to the [^{15}O]-H_2O PET and to the [^{18}F]-FDG PET template) were tested in a jack-knife approach, where every normalized [^{18}F]-FDG PET scan was evaluated with respect to the remaining sample via the two sample t-test in SPM5 (i.e., one control vs. remaining controls for the [^{15}O]-H_2O PET functional normalization procedure and one control vs. remaining controls for [^{18}F]-FDG PET functional normalization procedure). A statistical map, or SPM-t, was obtained for each of the two functional normalization procedure, estimating potential hypometabolic areas for each healthy subject, as compared to the remaining controls. Misclassified individuals were considered when cluster of voxels were present in the SPM-t with a minimum extent of 10 voxels and surviving at p<0.05 FWE-corrected threshold at a voxel level.

Single-Patient SPM Analysis

A single patient vs. healthy control group SPM analysis was performed for all considered [^{18}F]-FDG PET patient scans (23 AD/prodromal AD, 24 bvFTD and 20 DLB), for both the two functional normalization procedures.

Each single-patient [^{18}F]-FDG PET image was tested for relative 'hypometabolism' by comparison with normal controls on a voxel-by-voxel basis—using the two sample t-test design of SPM5. Age was included as a covariate. Due to the lack of any significant difference in metabolic activity of male

and female demented patients (Minoshima et al. 1997), gender was not controlled in the analysis.

Global normalization of voxel values used proportional scaling to a mean voxel value of 6.5 mg/100 mL/min. This value was derived from a previous study where it was successfully applied in SPM analysis for single subjects (see Signorini et al. (1999) for details). The grey matter threshold was left at the default 0.8 value (i.e., the mean brain intensity was computed from only those voxels with intensity above 0.8 of the mean over the entire scan). Additionally, voxel-wise comparisons were made using a within-brain comparison-specific explicit optimal threshold [^{18}F]-FDG mask created using the SPM masking toolbox (Ridgway et al. 2009) to produce average binary masks of the 113 [^{15}O]-H_2O-normalized or the 112 [^{18}F]-FDG-normalized control scans. This explicit mask was applied to restrict subsequent analyses to within-brain voxels, thus minimizing the contribution of the extra cerebral activity to the value of Cerebral Glucose Metabolism (CGM) (Spence et al. 2006).

The comparison between each single patient and the [^{15}O]-H_2O-normalized or the [^{18}F]-FDG-normalized control scans yielded two contrasts maps for patient testing for areas with relative decreases compared to the control population.

Subsequently, the analyses generated a *t* statistic for each voxel as specified by the linear contrast.

a. Hypometabolism: SPM-t approach

   SPM-t maps were generated to identify areas of significant hypometabolism (significant SPM-t). We investigated hypometabolic brain areas at a significance level of $p=0.05$, corrected for multiple comparisons with the family-wise error (FWE) option at the voxel level. Only clusters containing more than 100 voxels were considered to be significant (see Table 2).

b. Hypometabolism: ROI approach

   We used a region of interest (ROI) approach—by comparing statistical *t*-values extracted from SPM-t of hypometabolism in typical hypometabolic regions for each specific dementia condition. To obtain an unbiased estimate of hypometabolism from a priori ROIs associated with each of the three pathologies (i.e., AD or early AD, bvFTD and DLB), we created a 16 mm radius spherical ROI centered on the median reference x, y and z coordinates reported in previous investigations: the posterior cingulate cortex (PCC) for AD or prodromal AD (Anchisi et al. 2005; Teune et al. 2010; Chételat et al. 2003), the mid-ventral portion of the orbito-frontal gyrus (vmPFC) for bvFTD (Teune et al. 2010; Salmon et al. 2003), and the right middle occipital cortex (RmOC) for DLB (Teune et al. 2010; Mori et al. 2006).

   The closest local maxima to the reference x, y and z coordinates in the a priori pathology-specific brain region was selected with the Anatomy Toolbox (Eickhoff et al. 2005) in each single patient [^{18}F]-FDG SPM-t.

   Single voxel *t*-values within the a priori pathology-specific ROI were then extracted from SPM-t images following the [^{15}O]-H_2O PET and the [^{18}F]-FDG PET normalization procedures for each patient, while excluding all zero voxels from the ROI. This procedure enabled us to compare differences between *t*-values over voxels and over patients for the two normalization procedures, and to look at the distribution of *t*-values in some canonical regions of interest.

c. Hypometabolism: second level analysis for whole-brain pattern approach

   Single-patient hypometabolism contrast maps resulting from single-patient SPM analysis for each of the two functional normalization procedures, were statistically tested at group-level for disease-specific groups (only AD/prodromal AD, only bvFTD, and only DLB). Two separate one sample *t*-test designs in SPM5 were performed for each functional normalization procedures, applying a normalization-specific within-brain explicit mask (as previously described) with the purpose of identifying areas of hypometabolism common to all patients.

   For each of the two functional normalization procedures, group SPM-t maps were obtained representing disease-specific patterns of hypometabolism for AD/prodromal AD, for bvFTD and for DLB (Anchisi et al. 2005; Teune et al. 2010; Chételat et al. 2003; Salmon et al. 2003; Mori et al. 2006). These SPM-t maps were assessed at a threshold of $p<0.05$, FWE corrected for multiple comparisons at a voxel-level and a threshold for minimum spatial extent of ten contiguous voxels. The Anatomic Automatic Labeling software (AAL) (Tzourio-Mazoyer et al. 2002) was used for anatomical localization of statistically significant clusters.

   For visualization purposes only, we computed smoothed histograms (i.e., density plots) to quantify the degree of overlap/separation between the distribution of the voxel values over the whole-brain (see Fig. 5) in the 2nd level group hypometabolic contrast images resulting from the two normalization procedures ([^{15}O]-H_2O and [^{18}F]-FDG) in the three dementia subgroups.

d. Diagnostic effectiveness

   To assess the diagnostic performance of the use of the [^{18}F]-FDG PET template in detecting both disease-specific PET patterns and normality, we calculated sensitivity, specificity, area under the ROC curve (AUC) values and a global measure of diagnostic accuracy (i.e., effectiveness). This kind of analysis was applied to the entire cohort of patients and controls considered in the present context. Gold standard for True Positives and True Negatives was the confirmed diagnosis of neurologists at clinical follow-up (18 months after the first evaluation and 15 months after the PET studies).

Table 2 Reports coordinates, t-statistic values, cluster extents and labels in major brain anatomical subdivisions relevant for the classification of dementia forms and resulting from the single-subject-versus-group analysis comparing each of the four patients (AD, aMCI, bvFTD and DLB) to a database of normal controls implementing the spatial normalization procedure implemented with the standard [^{15}O]-H_2O template OR with the newly created dementia-specific [^{18}F]-FDG template

			[^{15}O]-H_2O PET template			[^{18}F]-FDG PET template			
	Major brain subdisions[a]	Left/Right	Local maxima (x,y,z)	t-statistic	Cluster extent (k_E)	Local maxima (x,y,z)	t–statistic	Cluster extent (k_E)	Atlas Label (AAL)[b]
SUBJECT 1 Alzheimer's Disease	Frontal cortex (ACC, VMPF, DLPF)	R	30 2 62	17.32	2247	26 0 66	**19.15**	13403*	*Middle frontal gyrus*
		L/R	4 10 42	7.06	2213	2 10 42	**8.73**	*	*Middle cingulate cortex*
		L	−34 4 60	16.95	2213	−34 0 62	**17.55**	*	*Middle frontal gyrus*
	Temporal Cortex (Pole, mesial and lateral)	R	–	–	–	*60 −46 −10*	*6.85*	*22335***	*Inferior temporal gyrus*
		L	–	–	–	*−42 −14 −32*	*7.77*	*239*	*Inferior temporal gyrus*
		L	−62 −46 −20	9.47	270	−60 −46 −20	**10.78**	**	*Inferior temporal gyrus*
	Parietal cortex (Superior and inferior)	R	38 −60 56	11.64	1745	36 −60 52	**18.1**	**	*Superior parietal lobule*
		L	−32−62 54	11.27	6557	−28−58 56	**14.37**	**	*Superior parietal lobule*
	PCC (Precuneus, PCC/ Retrosplenial)	R	–	–	–	–	–	–	–
		L	−8 −78 50	15.26	6557	−8 −74 54	**20.89**	**	*Precuneus*
	Occipital cortex (Lateral and medial)	R	–	–	–	–	–	–	–
		L	–	–	–	–	–	–	–
SUBJECT 2 amnestic MCI	Frontal cortex (ACC, VMPF, DLPF)	R	–	–	–	–	–	–	–
		L	*−46 42 −16*	*7.03*	*108*	–	*Orbitofrontal Gyrus*		
	Temporal Cortex (Pole, Mesial and Lateral)	R	–	–	–	–	–	–	–
		L	−56 −64 −16	**10.52**	186	−56 −68 −14	7.73	3894	*Inferior temporal gyrus*
		L	–	–	–	*−32 −12 −26*	*9.13*	*6107**	*Hippocampus*
	Parietal cortex (Superior and inferior)	R	–	–	–	*44 −74 44*	*14.95*	*	*Superior parietal lobule*
		L	–	–	–	*−32 −74 46*	*11.82*	*	*Inferior parietal lobule*
	PCC (Precuneus, PCC/ Retrosplenial)	R	6 −60 64	7.64	362	8 −60 66	**12.14**	*	*Precuneus*
		L	−4 −46 24	10.25	581	−4 −44 26	**10.79**	*	*PCC*
	Occipital cortex (Lateral and medial)	R	–	–	–	–	–	–	–
		L	–	–	–	–	–	–	–
SUBJECT 3 bvFTD	Frontal cortex (ACC, VMPF, DLPF)	R	42 16 52	16.95	3814*	42 14 52	**17.43**	19332*	*Middle frontal gyrus*
		R	58 18 4	12.34	734	40 24 −2	**13.66**	*	*Frontal operculus*
		L/R	6 34 36	9.78	*	8 34 36	**11.48**	*	*ACC*
		L	−44 16 44	12.77	288	−44 22 42	**12.2**	*	*Middle frontal gyrus*
		L	−38 22 −6	13.34	890	−38 22 −6	**15.38**	*	*Inferior frontal gyrus*
	Temporal Cortex (Pole, Mesial and Lateral)	R	–	–	–	–	–	–	–
		L	–	–	–	–	–	–	–
	Parietal cortex (Superior and inferior)	R	–	–	–	–	–	–	–
		L	–	–	–	–	–	–	–
		R	–	–	–	–	–	–	–

Table 2 (continued)

	Major brain subdisions[a]	Left/Right	[^{15}O]-H_2O PET template			[^{18}F]-FDG PET template			
			Local maxima (x,y,z)	t-statistic	Cluster extent (k_E)	Local maxima (x,y,z)	t–statistic	Cluster extent (k_E)	Atlas Label (AAL)[b]
	PCC (Precuneus, PCC/ Retrosplenial)	L	–	–	–	–	–	–	–
	Occipital cortex (Lateral and medial)	R	–	–	–	–	–	–	–
		L	–	–	–	–	–	–	–
SUBJECT 4 DLB	Frontal cortex (ACC, VMPF, DLPF)	R	–	–	–	–	–	–	–
		L	–	–	–	*−28 18 −24*	*7.93*	*170*	*Inferior frontal gyrus*
		L	–	–	–	*−46 38 18*	*10.99*	*304*	*Inferior frontal gyrus*
	Temporal Cortex (Pole, Mesial and Lateral)	R	58 −62 −16	8.94	668	58 −62 −16	**13.4**	30662*	*Inferior temporal gyrus*
		L	−56 −56 −20	10.39	2733	−60 −54 −12	**15.13**	*	*Inferior temporal gyrus*
	Parietal cortex (Superior and inferior)	R	48 −64 36	10.61	1592	48 −64 38	**15.02**	*	*Inferior parietal lobule*
		L	−40 −62 44	8.39	1985	−48 −58 46	**14.15**	*	*Inferior parietal lobule*
	PCC (Precuneus, PCC/ Retrosplenial)	R	–	–	–	*2 −58 14*	*8.61*	*	*PCC*
		L	–	–	–	–	–	–	–
	Occipital cortex (Lateral and medial)	R	30 −90 24	12.57	1592	32 −90 20	**17.39**	*	*Middle occipital gyrus*
		L	−30 86 26	11.15	1985	−32 −86 26	**17.53**	*	*Middle occipital gyrus*

The two procedures ([^{15}O]-H_2O and [^{18}F]-FDG) are here compared in terms of both hypometabolic pattern and statistical outcomes at the single-subject level in the following manner: first, clusters of hypometabolism in the SPM-t thresholded at p=0.05 (FWE corrected) at the voxel level and with a minimum size of 100 voxels following the standard [^{15}O]-H_2O normalization procedure for each patient were highlighted in each brain subdivision; t-statistic values and cluster extents resulting from the standard [^{15}O]-H_2O procedure were set as a reference for the [^{18}F]-FDG procedure; second, clusters of hypometabolism in the SPM-t thresholded at p=0.05 (FWE-corrected) at the voxel level and with a minimum size of 100 voxels following the [^{18}F]-FDG normalization procedure for each patient were highlighted; local maxima (in a range of 10 mms on x, y or z) were identified at the same peak coordinates of all clusters reported in the brain subdivisions with the standard [^{15}O]-H_2O procedure; t-statistic values and cluster extents are reported for each local maxima. Clusters found to be significant in the relevant brain subdivisions following ONE normalization procedure but not the other are reported in Italic. Higher t-statistical values following ONE normalization procedure but not the other are instead reported in BOLD

*The asterisks indicate local maxima included in the same cluster. Cluster extent (k_E) indicates the number of voxels included in the cluster. Values in BOLD indicate a higher t-statistic. Values in Italic indicate local maxima resulting specifically from ONE of the two procedures

[a] These major brain anatomical areas correspond to subdivisions particularly relevant for the classification of dementia forms in terms of hypometabolic [^{18}F]-FDG PET patterns

[b] The AAL (Automated Anatomical Labelling) digital atlas of the human brain was used for localizing and labelling clusters of significant hypometabolism in the different major brain subdivisions

Results

[^{18}F]-FDG PET Template Creation

The visual inspection of normalized [^{18}F]-FDG PET image yielded a final set of 110 images (55 controls and 55 patients) after the exclusion of five pairs of control-patient images (due to convergence failures).

A matrix of distances between all pairs of images revealed the presence of outlier scans (see red values in the right panel of Fig. 1). In particular, the Cook test (testing for the influence of a particular scan on the average) showed that five scans deviated further than the critical D value (D=0.036) (see Fig. 1), leading to the exclusion of five matched pairs of control-patient images (ten scans).\

Figure 2 shows the difference in intensity within transaxial sections of the resulting [^{18}F]-FDG PET template (100 images) as compared to the standard [^{15}O]-H_2O template available in SPM 5 (12 images).

Validation of [^{18}F]-FDG PET Template

The final set of images included as a control group for the present study and normalized with the [^{15}O]-H_2O and with the [^{18}F]-FDG functional normalization procedure resulted in 113 and 112 images, respectively.

All images included as patients for the present study normalized with the [^{15}O]-H_2O and with the [^{18}F]-FDG functional normalization procedure included 67 images (23 AD/prodromal AD, 24 bvFTD and 20 DLB).

Assessment of "Normality" Rate

A false positive rate of 7 % was found for the control dataset normalized to [^{15}O]-H_2O template, while a false positive rate of 6 % was obtained for those normalized to [^{18}F]-FDG PET template. There was considerable overlap between the false positives obtained from the two normalization procedures (r= 0.56; p<0.001), speaking to the consistency between them. However, the false positives identified among healthy controls normalized to [^{15}O]-H_2O template showed a greater number of clusters with a larger extent with respect to those found among the [^{18}F]-FDG-normalized ones (see supplementary Table 1).

Single-Patient SPM Analysis

a. Hypometabolism: SPM-t approach

Results for four patients representative of different dementia conditions are shown in Fig. 3.

In all four dementia cases (AD, amnesic MCI, bvFTD and DLB patient), the single-patient analysis, based on the comparison of SPM-t maps from the two normalization procedures, revealed: a) higher local maxima peak values (t-statistic) and b) larger Cluster Extent (K_E, number of voxels) when image normalization to the [^{18}F]-FDG PET template was used, highlighting a more extensive hypometabolic pattern (see Fig. 3 and Table 2 for details). In particular:

SPM-t maps of the AD patient showed a bilateral temporo-parietal hypometabolism, particularly involving the precuneus, inferior and superior parietal cortex. Hypometabolic regions were more extended when the subject was normalized to the [^{18}F]-FDG PET template. The [^{18}F]-FDG PET normalization yielded higher statistical sensitivity and revealed significant hypometabolic clusters, not present in the SPM-t generated following the [^{15}O]-H_2O normalization (see Fig. 3a, and Table 2 panel A).

SPM-t maps of the amnesic MCI patient, after the [^{18}F]-FDG PET normalization procedure, showed a hypometabolic pattern typical of AD pathology, involving temporo-parietal cortex bilaterally, and in addition, the left

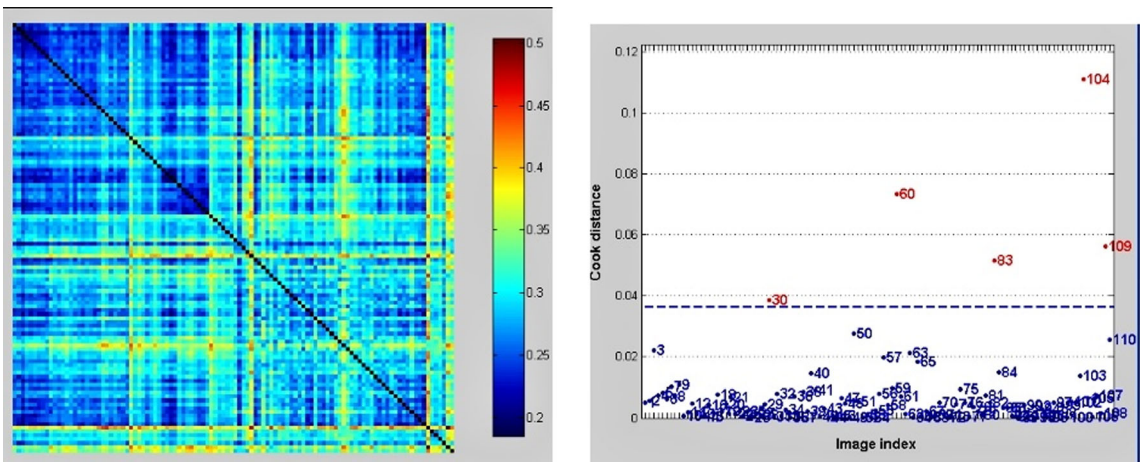

Fig. 1 On the left panel, the matrix of distances between all scans (55 controls and 55 patients). On the *right panel*, the Cooks distance revealing the outlier images (*red values*) with larger values than the critical D value, which were excluded from the final set of images

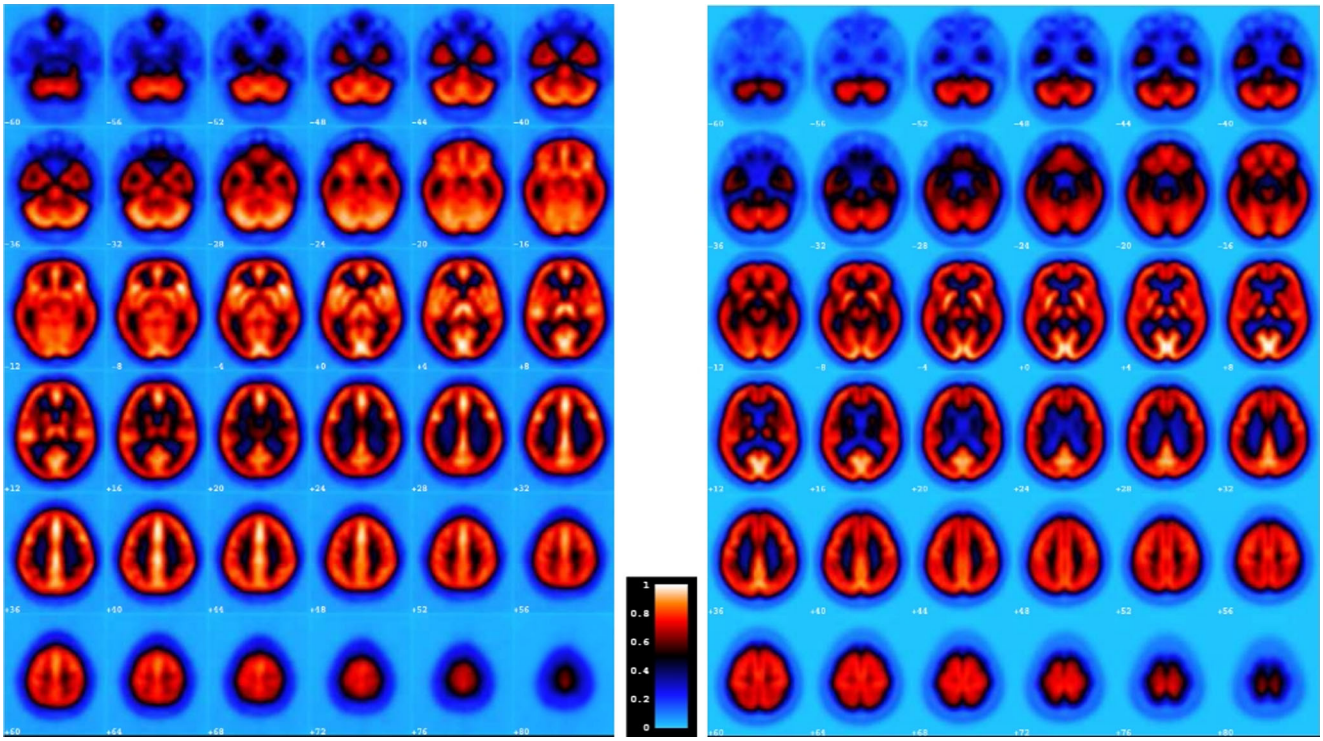

Fig. 2 Standard [15O]-H2O PET template provided with SPM5 (*left panel*); [^{18}F]-FDG PET Template built by averaging normalized [^{18}F]-FDG PET images (*right*). Axial slices are ordered from bottom to top and the slices are 4 mms apart

hippocampus, posterior cingulate cortex (PCC) and precuneus (see Table 2B and Fig. 3 panel B). The same patient, following the [^{15}O]-H_2O normalization procedure, showed only two significant clusters—located in the inferior temporal gyrus and in the precuneus/PCC. The anterior hypometabolic cluster highlighted in the frontal lobe following the [^{15}O]-H_2O normalization procedure was located at the edges of the orbito-frontal cortex, revealing a potential misregistration artifact. This artifact disappeared using [^{18}F]-FDG PET template.

SPM-t maps of the bvFTD patient showed an hypometabolic pattern of bilateral prefrontal dysfunction, which was significantly larger when using the [^{18}F]-FDG normalization instead of the [^{15}O]-H_2O normalization (see Fig. 3c, and Table 2 panel C).

SPM-t maps of the DLB patient showed a more extended metabolic decrease with the [^{18}F]-FDG normalization, involving temporal, occipital and parietal regions, the typical hypometabolic pattern observed in DLB. The SPM following the [^{18}F]-FDG normalization also pinpointed a frontal hypometabolism not observed with the [^{15}O]-H_2O procedure, also part of the typical DLB pattern (see Fig. 3d, and Table 2 panel D).

FDG-PET scans for three patients acquired with a different scanner from those used to build the [^{18}F]-FDG template and spatially normalized following the [^{18}F]-FDG normalization or the [^{15}O]-H2O procedure also underwent single-subject analysis in order to assess differences between the resulting hypometabolic patterns. (see supplementary material and Figure S1 for details).

b. Hypometabolism: ROI approach

Figure 4a (left panel) shows the SPM-t values, obtained following the [^{15}O]-H_2O (green color) and [^{18}F]-FDG (blue color) normalization procedure, for each voxel falling within the pathological-specific ROIs. SPM-t values are averaged over the group population (23 AD/early AD patients in the upper part of the figure, 24 bvFTD in the middle part and 20 DLB patients in the lower part). For all groups of patients, the SPM-t values are higher after the [^{18}F]-FDG normalization.

Figure 4b (middle panel), shows the difference plot (Bland-Altman plot) between the SPM-t values, obtained following the two normalization procedures for each patient of the different dementia subgroup. The difference values are averaged over voxels within the pathology-specific ROI. The plot establishes that the mean difference between t-values from the two normalization procedures is substantially shifted away from 0 when plotted against the average t-values from the two procedures.

Figure 4c (right panel), shows the distribution of the SPM-t values, averaged over the group population and over the pathological-specific ROI voxels. As one can observe, they are more statistically significant when using the [^{18}F]-FDG procedure.

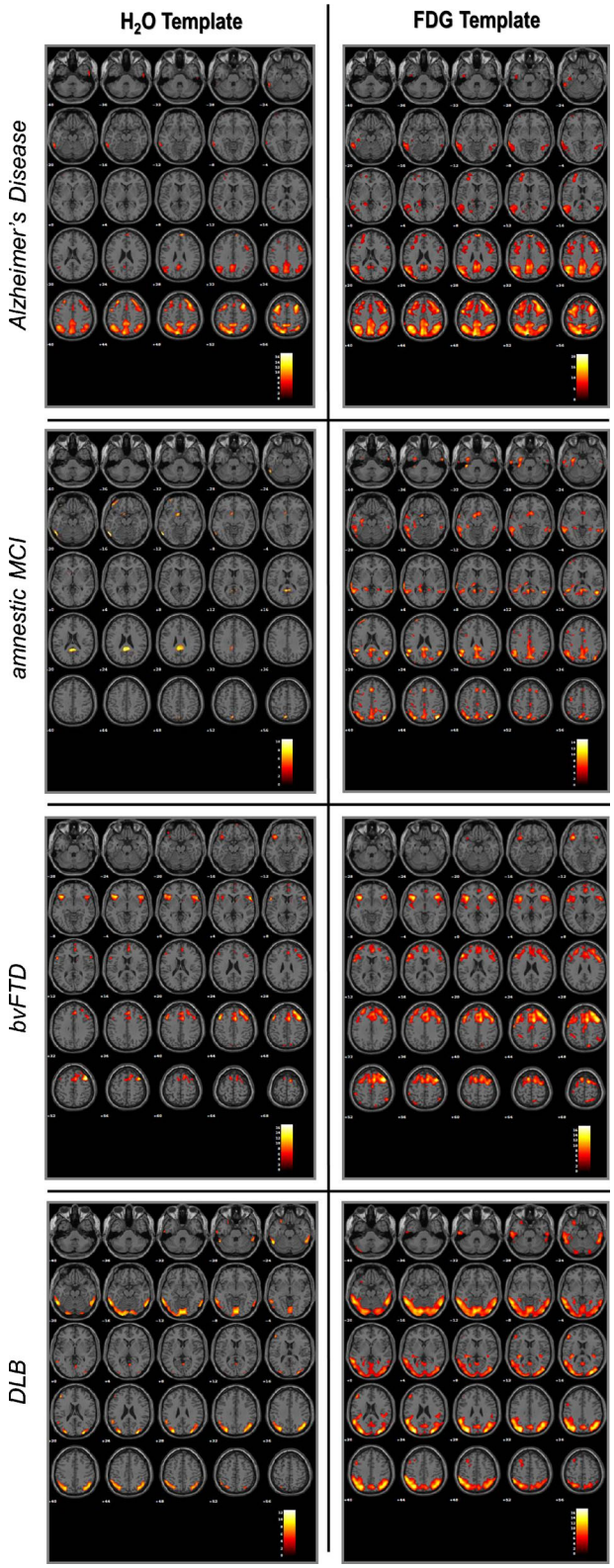

Fig. 3 Single-patient SPM hypometabolic maps overlaid on the structural MNI single- subject template included in SPM5. For each panel the left part displays the pattern of hypometabolism following the [^{15}O]-H_2O normalization procedure; the right part displays the pattern of hypometabolism following the [^{18}F]-FDG PET normalization procedure. In all four cases, statistical outcomes after the normalization procedure implemented with the [^{18}F]-FDG PET template reveal higher local maxima peak values (t-stastitics) and larger cluster extents with respect to the standard [^{15}O]-H_2O normalization procedure (see Table 2 for details)

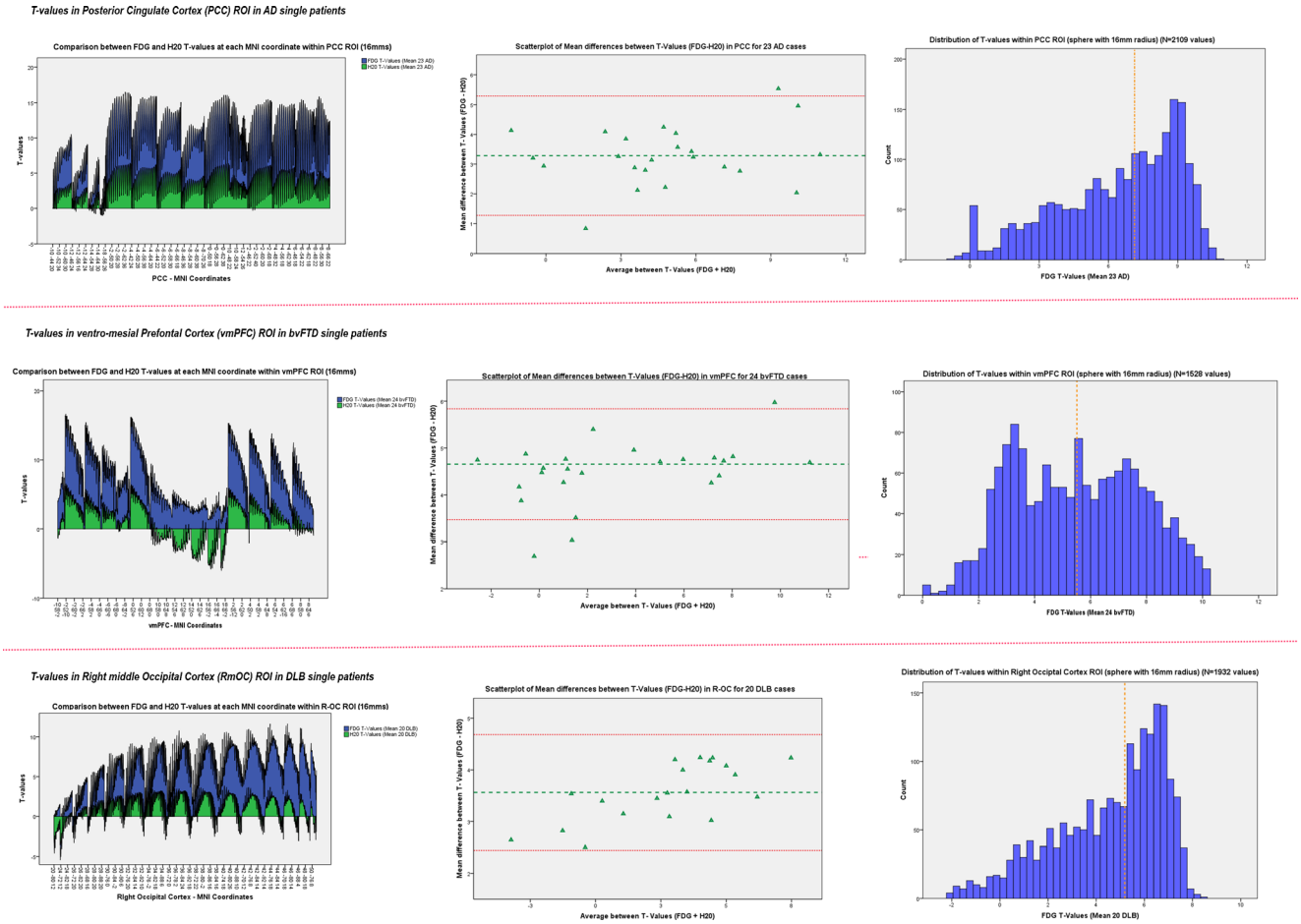

Fig. 4 Plots and distribution of t-values over voxels and over subjects in predefined ROIs for 23 AD (*top row*), 24 bvFTD (*middle row*) and 20 DLB (*bottom row*) patients. The *bar-plots* in the *left panel* show the comparison between the height of t-values (y axis) in single voxels extracted at all coordinates (x-axis) contained within the 16 mm spherical ROI following [^{15}O]-H_2O (*green*) or [^{18}F]-FDG (*blue*) normalization procedures and averaged over all patients for each dementia sub-type. The graphs in the *middle panel* display a scatter diagram of the differences (y-axis) plotted against the averages of the t-values (x-axis) following the [^{18}F]-FDG and the [^{15}O]-H_2O normalization procedures for each patient. *Horizontal lines* are drawn at the mean difference (*green line*), and at the limits of agreement (*red lines*), which are defined as the mean difference plus and minus 1.96 times the standard deviation of the differences. This difference plot allowed us to compare the two normalization procedures in order to establish if the mean difference in t-values between the two procedures (plotted against their averages) is significant in terms of the amount of shift with respect to 0 with respect to the difference observed in the ROI for each single patient. The histograms in the *right panel* show the distribution and the median (*orange line*) of the empirical T distributions of single voxel t-values extracted from SPM-T maps following the [^{18}F]-FDG normalization procedure and averaged over all patients in each dementia sub-group

c. Hypometabolism: Second level analysis for whole-brain pattern approach

Disease-specific patterns of hypometabolism at the group level, following single patient SPM analysis with spatial normalization to the [^{15}O]-H_2O template or to the [^{18}F]-FDG template, were different for all three dementia subtypes (see Table 3 and Fig. 5).

In the AD/prodromal AD group, a more widespread pattern was detected following the [^{18}F]-FDG normalization involving, bilaterally, the precuneus, the mid-posterior cingulate cortex and extensively the parietal lobes (see Table 3 for exact coordinate peaks and localization).

In bvFTD group, the [^{18}F]-FDG normalized hypometabolic pattern included the superior portion of the medial frontal gyrus and anterior cingulate cortex—extending to the middle and inferior parts of orbito-frontal gyrus, and bilaterally to the insular cortices involving the pars orbitalis, triangularis and opercularis of the inferior frontal gyrus to a greater extent with respect to [^{15}O]-H_2O-normalized hypometabolic group SPM (see Table 3 for exact coordinate peaks and localization).

For the DLB group, the hypometabolic pattern following normalization to the [^{18}F]-FDG template comprised the inferior, middle and superior occipital cortices, extending dorsally to the parietal lobes and the precuneus bilaterally, while [^{15}O]-H_2O-

Table 3 reports coordinates, t-statistic values, cluster extents and AAL labels resulting from SPM group analysis of hypometabolic contrast estimates on AD (n=23), bvFTD (n=24) and DLB (n=20) cases following the two spatial normalization procedures implemented with the standard [^{15}O]-H_2O template OR with the newly created dementia-specific [^{18}F]-FDG template

Group	[^{15}O]H_2O Template			[^{18}F]FDG Template			Atlas label (AAL)[a]
	Local maxima (x,y,z)	t-statistic	Cluster extent (k_E)	Local maxima (x,y,z)	t-statistic	Cluster extent (k_E)	
GROUP 1 Alzheimer's Disease	2 -66 10	6.51	39	2 −68 28	12.53	3999	*L/R Precuneus*
	–	–	–	46 −64 28	11.08	2474	*R Angular Gyrus*
	–	–	–	−42 −66 36	10.20	2226	*L Angular Gyrus*
	–	–	–	*64 −36 −8*	*8.17*	*88*	*R Mid-temporal gyrus*
	–	–	–	*32 20 44*	*8.06*	*110*	*R Mid-frontal gyrus*
GROUP 2 bvFTD	0 54 0	6.36	27	2 56 0	10.75	2594	*L/R medial superior -orbito-frontal gyrus*
	36 36 −24	8.99	36	34 30 −26	10.08	529[b]	*R inferior orbito-frontal gyrus*
	52 20 −6	7.29	28	34 26 2	7.54	[b]	*R insula/inferior frontal gyrus*
	−36 30 −22	7.54	12	−38 14 −2	7.82	282	*L insula/inferior frontal gyrus*
	−28 46 −20	6.93	30	−22 30 −24	7.10	203	*L orbito-frontal gyrus*
	–	–	–	26 48 −22	7.18	16	*R orbito frontal gyrus*
	–	–	–	−18 52 38	7.54	106	*L superior and medial forntal gyrus*
	–	–	–	0 −16 6	7.79	45	*L/R thalamus*
GROUP 3 DLB	36 −68 42	7.30	66	34 −66 42	13.48	9328[b]	*R angular gyrus*
	−30 −70 32	7.59	32	−30 −84 −4	*12.18*	[b]	*L mid-inferior occipital cortex*
	–	–	–	*30 −72 34*	*13.13*	[b]	*R mid-superior occipital cortex*
	–	–	–	62 −40 −10	7.00	10	*R mid temporal gyrus*

The two procedures ([^{15} O]-H_2O and [^{18} F]-FDG) are here compared in terms of both hypometabolic pattern and statistical outcomes at the group level in the following manner: 1) Clusters of hypometabolism in the SPM-t thresholded at p=0.05 (FWE corrected) at the voxel level and with a minimum size of 10 voxels following the standard [^{15} O]-H_2O normalization procedure (left) and for the [^{18} F]-FDG procedure (right); 2) Local maxima for each brain area (in a range of 10mms on x, y or z) were identified at the specific peak coordinates for each normalization procedure; t-statistic values and cluster extents are reported for each local maxima

[a] The AAL (Automated Anatomical Labeling) digital atlas of the human brain was used for localizing and labeling clusters of significant hypometabolism in the different major brain subdivisions

[b] The asterisks indicate local maxima included in the same cluster. (k_E) (cluster extent) indicates the number of voxels included in the cluster

normalized hypometabolism was limited to two small clusters at parietal sites (see Table 3 for exact coordinate peaks and localization).

Inspection of the density plots (see Fig. 5) reveals a considerable separation between hypometabolic mean contrast estimate values with higher values for [^{18}F]-FDG normalization as compared to [^{15}O]-H_2O normalization. They reveal a similar pattern of dispersion around the mean for the AD (i.e., [^{18}F]-FDG=0.02±0.80 and [^{15}O]-H_2O=−1.01±0.82), bvFTD (i.e., [^{18}F]-FDG=−0.22±0.88 and [^{15}O]-H_2O=−1.32±0.94) and DLB (i.e., [^{18}F]-FDG=−0.03±0.92 and [^{15}O]-H_2O=−1.11±0.93) groups.

d. Diagnostic effectiveness

SPM-ts following the [^{18}F]-FDG normalization procedure performed excellently at discriminating between the three dementia subtype and normality (AUC=0.93; sensitivity 91 %; specificity 95 %) (see Fig. 6), yielding 94 % of diagnostic accuracy, expressed as the proportion of correctly classified subjects (i.e. True Positives + True Negatives) among all subjects (i.e. True Positives + True Negatives + False Positives + False Negatives).

Discussion

We constructed an [^{18}F]-FDG PET dementia-specific template from images obtained from multiple centers. We then validated the use of this new template in spatial normalization—as a prerequisite for statistical comparison of normal and dementia subjects—while controlling for differences due to different scanner characteristics or data-acquisition protocols.

The validity of the spatial normalization with the new [^{18}F]-FDG PET template was evaluated against that with the [^{15}O]-H_2O PET template in patients affected by different forms of dementia. We demonstrated that use of a

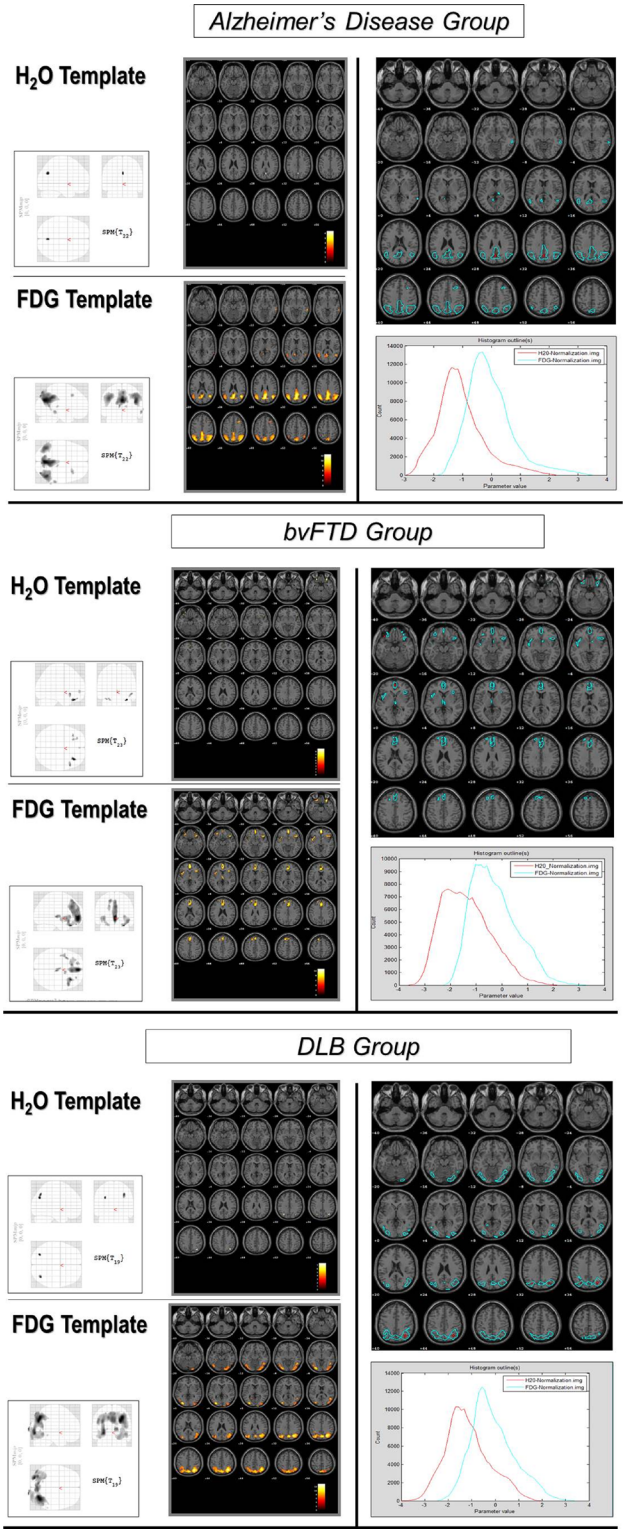

Fig. 5 Group SPMs of hypometabolism for 3 dementia subtypes (i.e., AD, bvFTD and DLB). For each group panel the left parts display the pattern of hypometabolism shown on SPM glass brain and overlaid on the structural MNI single-subject template included in SPM5 following the [^{15}O]-H_2O normalization procedure (upper portion) or the [^{18}F]-FDG PET normalization procedure (*bottom portion*); the upper right part displays the contours of the pattern of hypometabolism following the [^{15}O]-H_2O normalization procedure (*red*) or the [^{18}F]-FDG PET normalization procedure (cyan). The *bottom right* part shows the smoothed histograms (i.e., density plots) of the distribution of the voxel values over the whole-brain. The values refer to the contrast estimates of hypometabolism at the group level following the [^{18}F]-FDG-normalization procedure or the [^{15}O]-H_2O normalization procedure

population-specific [^{18}F]-FDG PET template can improve the sensitivity of statistical inferences about brain metabolism, in terms of both levels of statistical significance and the size of significant clusters detected.

We propose that this new template could be useful for both research and clinical purposes, allowing the detection of subtle metabolic abnormalities associated with specific cognitive impairment and the recognition of different patterns of neurodegeneration—particularly at the single-subject level and in early disease stages (see Fig. 3). The validity of single-subject analyses was assessed through their consistency with the established relationship between dementia subtypes and hypometabolic patterns (see Fig. 3 and Table 2). Improved statistical power using the new [^{18}F]-FDG PET template was confirmed by distributional differences in the final *t*-statistics testing for single subject effects in a priori pathology-specific ROIs, over a cohort of patients (n>20) for each dementia subtype (Fig. 4).

Our findings in the amnesic MCI subject (see Table 2 and Fig. 3, panel B) further suggest that the normalization of [^{18}F]-FDG PET images from pathological brains using the existing [^{15}O]-H_2O PET template is a potential source of error. The [^{18}F]-FDG PET normalization procedure identified the typical AD metabolic pattern and a clear involvement of the hippocampus and posterior cingulate cortex (see Table 2 and Fig. 3, panel B). These differences were not evident in the SPM with the [^{15}O]-H_2O normalization procedure. Thus, the sensitivity to differences in specific brain regions involved in neurodegenerative processes (i.e., hippocampus, inferior temporal and occipital regions) seems to be affected by the quality of spatial normalization (Krishnan et al. 2006; Rorden et al. 2012).

Our results suggest that the [^{18}F]-FDG PET template provides a higher degree of accuracy, for spatial normalization of [^{18}F]-FDG PET scans. Precise anatomical registration of regional metabolic changes enables voxel by voxel analyses, which has fundamental advantages over visual assessment. To increase diagnostic reliability in early phases of the disease process and make statistically informed decisions about metabolic abnormalities associated with dementia, it is important to increase normalization accuracy in order to reduce random effects due to noise present in individual images, which is especially prevalent in PET (Markiewicz et al. 2009).

Our group analyses revealed higher statistical sensitivity with normalization to the [^{18}F]-FDG PET dementia-specific template, in relation to the existing [^{15}O]-H_2O normalization procedure (see Fig. 5) in areas with typically decreased glucose metabolism in AD (Herholz et al. 2002; Teune et al. 2010; Chételat et al. 2003), bvFTD (Teune et al. 2010; Salmon et al. 2003) and DLB (Teune et al. 2010; Minoshima et al. 2001). With respect to the DLB group, occipital hypometabolism has been shown to be a specific topographical marker of this dementia subtype (Minoshima et al. 2001); associated with DLB-specific clinical symptoms, such as visual hallucinations (Mori et al. 2006) that play a key role in the differential diagnosis with respect to AD (McKeith et al. 2005).

The new [^{18}F]-FDG PET template may be useful for clinical research by providing more effective discrimination

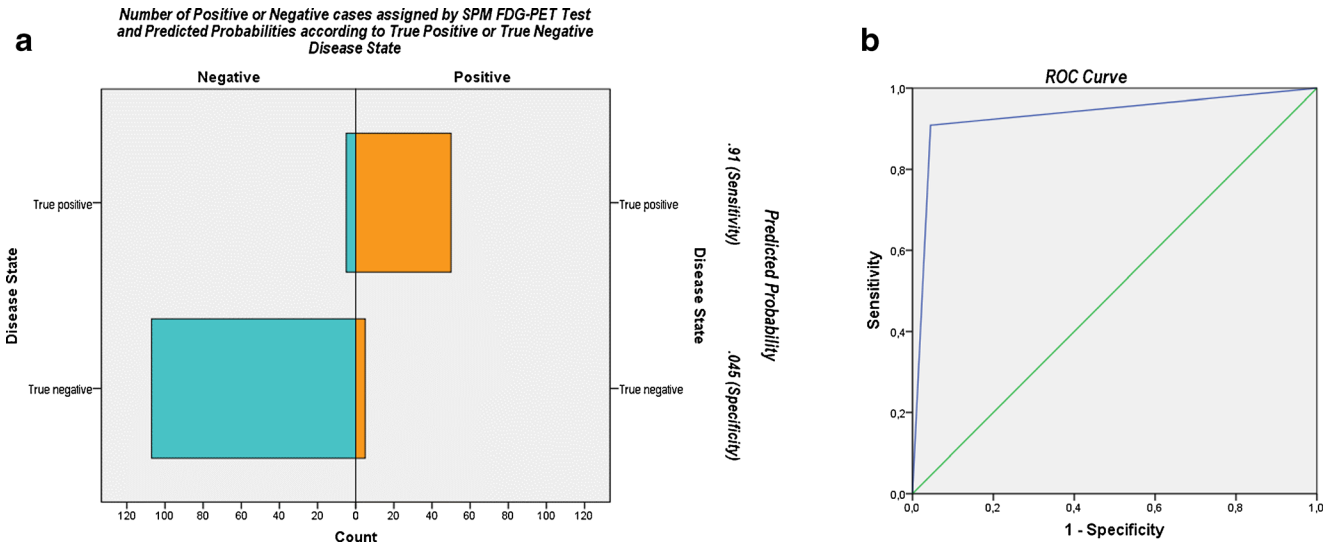

Fig. 6 **a** Plot of the cross-classification of binary SPM evaluation outcomes (1=positive, 0=negative for DLB—as evaluated by a neurologist according to the presence/absence of a typical disease-specific FDG-PET pattern of hypometabolism in a voxel-based SPM study, p<0.05, FWE corrected for multiple comparisons generated following normalization with the FDG-template) with the true category to which the subject belongs to, according to disease state (1=True Positive: presence of a true disease state; 0=True Negative: absence of a true disease state). The predicted classification probabilities (Sensitivity and 1-Specificity) are obtained from logistic regression of single-case binary response outcomes on category membership for true PRESENCE or ABSENCE of the disease. **b** Area under the ROC curve (AUC) as a result of plotting Sensitivity (one Highest True Positive probability value: p=0.91) against 1-Specificity (one Lowest False Positive probability value: p=0.045), resulting from the logistic regression of binary SPM evaluation outcomes on true PRESENCE or ABSENCE of disease state

between patient groups, particularly at early disease stages (see Fig. 5), allowing one to establish more clear-cut anatomo-clinical correlations (Teune et al. 2010). The [^{18}F]-FDG PET template may further help in research studies of atypical dementia or in subjects at risk for dementia with the intent to relate specific or subtle hypometabolic patterns, as revealed by SPM, to diverse neuropsychological pictures characterized by precise clinical symptoms.

We evaluated the ability of the new template to help differentiate between various disease conditions and the normal population. We thus determined its diagnostic accuracy using longitudinal clinical assessment of at least 18 months for patients as a gold standard, and a large sample of healthy subjects (n=112). Classification of patients and healthy controls, through SPM-t of hypometabolism, revealed an overall diagnostic accuracy of 94 %. This is in line with accuracies reported for other semi-quantitative measures (see for example Foster et al. (2007) reporting a diagnostic accuracy of 93 %).

Finally, some limits of spatial normalization have to be considered. In cases of severe atrophy, even when the PET image is matched to a bespoke reference template, particular attention is required in the interpretation of statistically significant areas of hypometabolism—specifically in relation to structural information. MRI-aided spatial normalization can be more accurate than normalization based only on functional images (Ashburner and Friston 1999; Martino et al. 2013), given the better anatomical information and higher spatial resolution. However, many clinical and research protocols for evaluation of dementia include PET imaging but do not necessarily involve MRI, which is necessary for MRI-based spatial normalization in single individuals. In these conditions, an accurate spatial normalization can be achieved by using the dementia-specific FDG-PET template presented here.

Furthermore, when studying neurodegenerative diseases where structural variability is profoundly increased by the underlying neurodegenerative processes, the use of the dementia-specific FDG-PET template for spatial normalization can provide two main benefits: 1) the spatial scale of metabolic anatomy is retained in the template, 2) normal and pathological functional anatomy are both defined operationally by regional glucose metabolism in this template.

In conclusion, we have contributed to optimize the application of SPM to analyze [^{18}F]-FDG PET images in research and the clinical setting.

Information Sharing Statement

The [^{18}F]-FDG-PET template presented here will be made available to download in the "Templates" section (http://www.fil.ion.ucl.ac.uk/spm/ext/#tpl) on the SPM (RRID :nif-0000-00343) official website (http://www.fil.ion.ucl.ac.uk/spm/) through the following URL: http://inlab.ibfm.cnr.it/PET_template.php

Acknowledgments We thank the EADC-PET Consortium (Alexander Drzezga and Robert Perneczky [Munich], Mira Didic and Eric Guedj [Marseilles], Bart N. Van Berckel and Rik Ossenkoppele [Amsterdam], Flavio Nobili and Silvia Morbelli [Genoa], Giovanni Frisoni, Anna Caroli [Brescia]) for kindly providing EADC-PET imaging data for the purposes of the current study. This study was supported in part by the 6th European Framework Program Network of Excellence "DIMI" LSHB-CT-2005-512146, and the 7th Framework Programme for Research and Technological Development "DECIDE" RI-261593 and in part by the Italian Ministry of Education in the framework of the Project of Strategic National Interest "Invecchiamento: innovazioni tecnologiche e molecolari per un miglioramento della salute dell'anziano" allocated to the National Research Council. Karl Friston and John Ashburner are based at The Wellcome Trust Centre for Neuroimaging, which is supported by core funding from the Wellcome Trust [091593/Z/10/Z].

Conflict of Interest The authors declare that they have no conflict of interest.

References

Albert, M. S., DeKosky, S. T., Dickson, D., Dubois, B., Feldman, H. H., Fox, N. C., et al. (2011). The diagnosis of mild cognitive impairment due to Alzheimer's disease: recommendations from the National Institute on Aging–Alzheimer's Association workgroups on diagnostic guidelines for Alzheimer's disease. *Alzheimer's & Dementia, 7*(3), 270–279.

Anchisi, D., Borroni, B., Franceschi, M., Kerrouche, N., Kalbe, E., Beuthien-Beumann, B., Cappa, S., et al. (2005). Heterogeneity of brain glucose metaboism in mild cognitive impairment and clinical progression to Alzheimer disease. *Archives of Neurology, 62*(11), 1728–1733.

Ashburner, J. (2007). A fast diffeomorphic image registration algorithm. *NeuroImage, 38*(1), 95–113.

Ashburner, J., & Friston, K. J. (1999). Nonlinear spatial normalization using basis functions. *Human Brain Mapping, 7*(4), 254–266.

Bartenstein, P., Asenbaum, S., Catafau, A., Halldin, C., Pilowski, L., Pupi, A., et al. (2002). European Association of Nuclear Medicine procedure guidelines for brain imaging using [(18)F]FDG. *European Journal of Nuclear Medicine and Molecular Imaging, 29*(10), BP43–BP48.

Berti, V., Osorio, R. S., Mosconi, L., Li, Y., De Santi, S., & de Leon, M. J. (2010). Early detection of Alzheimer's disease with PET imaging. *Neurodegenerative Diseases, 7*(1–3), 131–135.

Bornebroek, M., & Bretelera, M. B. (2004). Epidemiology of non-AD dementia. *Clinical Neuroscience Reserach, 3*, 349–361.

Buchert, R., Wilke, F., Chakrabarti, B., Martin, B., Brenner, W., Mester, J., & Clausen, M. (2005). Adjusted scaling of FDG positron emission tomography images for statistical evaluation in patients with suspected Alzheimer's disease. *Journal of Neuroimaging, 15*, 348–355.

Caroli, A., Prestia, A., Chen, K., Ayutyanont, N., Landau, S. M., Madison, C. M., et al. (2012). Summary metrics to assess Alzheimer disease-related hypometabolic pattern with 18F-FDG

PET: head-to-head comparison. *Journal of Nuclear Medicine, 53*(4), 592–600.

Chételat, G., Desgranges, B., de la Sayette, V., Viader, F., Eustache, F., & Baron, J. C. (2003). Mild cognitive impairment: Can FDG-PET predict who is to rapidly convert to Alzheimer's disease? *Neurology, 60*(8), 1374–1377.

Crivello, F., Schormann, T., Tzourio-Mazoyer, N., Roland, P. E., Zilles, K., & Mazoyer, B. M. (2002). Comparison of spatial normalization procedures and their impact on functional maps. *Human Brain Mapping, 16*(4), 228–250.

Dubois, B., Feldman, H. H., Jacova, C., Cummings, J. L., Dekosky, S. T., Barberger-Gateau, P., et al. (2010). Revising the definition of Alzheimer's disease: a new lexicon. *Lancet Neurology, 9*(11), 1118–1127.

Eickhoff, S., Stephan, K. E., Mohlberg, H., Grefkes, C., Fink, G. R., Amunts, K., et al. (2005). A new SPM toolbox for combining probabilistic cytoarchitectonic maps and functional imaging data. *NeuroImage, 25*(4), 1325–1335.

Evans, A. C., Collins, D. L., Mills, S. R., Brown, E. D., Kelly, R. L., & Peters, T. M. (1993). 3D statistical neuroanatomical models from 305 MRI volumes. *IEEE-Nuclear Science Symposium and Medical Imaging Conference Proceeding*, 1813–1817.

Foster, N. L., Heidebrink, J. L., Clark, C. M., Jagust, W. J., Arnold, S. E., Barbas, N. R., et al. (2007). FDG-PET improves accuracy in distinguishing frontotemporal dementia and Alzheimer's disease. *Brain, 130*(Pt10), 2616–2635.

Friston, K. J., Holmes, A. P., Worsley, K. J., Poline, J. P., Frith, C. D., & Frackowiak, R. S. (1994). Statistical parametric maps in functional imaging: a general linear approach. *Human Brain Mapping, 2*(4), 189–210.

Gispert, J. D., Pascau, J., Reig, S., Martinez-Lazaro, R., Molina, V., Garcia-Barreno, P., et al. (2003). Influence of the normalization template on the outcome of statistical parametric mapping of PET scans. *NeuroImage, 19*(3), 601–612.

Good, C. D., Johnsrude, I. S., Ashburner, J., Henson, R. N., Friston, K. J., & Frackowiak, R. S. (2001). A voxel-based morphometric study of ageing in 465 normal adult human brains. *NeuroImage, 14*(1 Pt1), 21–36.

Herholz, K., Salmon, E., Perani, D., Baron, J.-C., Holthoff, V., Frölich, L., Schönknecht, P., et al. (2002). Discrimination between Alzheimer dementia and controls by automated analysis of multicenter FDG PET. *NeuroImage, 17*(1), 302–316.

Ishii, K., Willoch, F., Minoshima, S., Drzezga, A., Ficaro, E. P., Cross, D. J., et al. (2001). Statistical brain mapping of 18F-FDG PET in Alzheimer's disease: validation of anatomic standardization for atrophied brains. *Journal of Nuclear Medicine, 42*(4), 548–557.

Jack, C. R., Jr., Albert, M. S., Knopman, D. S., McKhann, G. M., Sperling, R. A., Carrillo, M. C., et al. (2011). Introduction to the recommendations from the National Institute on Aging–Alzheimer's Association workgroups on diagnostic guidelines for Alzheimer's disease. *Alzheimer's & Dementia, 7*(3), 257–262.

Kherif, F., Poline, J. P., Mériaux, S., Benali, H., Flandin, G., & Brett, M. (2003). Group analysis in functional neuroimaging: selecting subjects using similarity measures. *NeuroImage, 20*(4), 2197–2208.

Krishnan, S., Slavin, M. J., Tran, T. T., Doraiswamy, P. M., & Petrella, J. R. (2006). Accuracy of spatial normalization of the hippocampus: implications for fMRI research in memory disorders. *NeuroImage, 31*(2), 560–571.

Magistretti, P. J. (2000). Cellular bases of functional brain imaging: insights from neuron-glia metabolic coupling. *Brain Research, 886*(1–2), 108–112.

Markiewicz, P. J., Matthews, J. C., Declerck, J., & Herholz, K. (2009). Robustness of multivariate image analysis assessed by resampling techniques and applied to FDG-PET scans of patients with Alzheimer's disease. *NeuroImage, 46*(2), 472–485.

Martino, M. E., Guzman de Villoria, J., Lacalle-Aurioles, M., Olazaran, J., Cruz, I., Navarro, E., et al. (2013). Comparison of different methods of spatial normalization of FDG-PET brain images in the voxel-wise analysis of MCI patients and controls. *Annals of Nuclear Medicine*. doi:10.1007/s12149-013-0723-7.

McKeith, I. G., Dickson, D. W., Lowe, J., Emre, M., O'Brien, J. T., Feldman, H., et al. (2005). Diagnosis and management of dementia with Lewy bodies: third report of the DLB Consortium. *Neurology, 65*(12), 1863–1872.

McKhann, G. M., Albert, M. S., Grossman, M., Miller, B., Dickson, D., & Trojanowski, J. Q. (2001). Clinical and pathological diagnosis of frontotemporal dementia: report of the Work Group on Frontotemporal Dementia and Pick's Disease. *Archives of Neurology, 58*, 1803–1809.

McKhann, G. M., Knopman, D. S., Chertkow, H., Hyman, B. T., Jack, C. R., Jr., Kawas, C. H., Klunk, W. E., et al. (2011). The diagnosis of dementia due to Alzheimer's disease: recommendations from the National Institute on Aging– Alzheimer's Association workgroups on diagnostic guidelines for Alzheimer's disease. *Alzheimer's & Dementia, 7*(3), 263–269.

Minoshima, S., Frey, K. A., Koeppe, R. A., Foster, N. L., & Kuhl, D. E. (1995). A diagnostic approach in Alzheimer's disease using three-dimensional stereotactic surface projections of fluorine-18-FDG PET. *Journal of Nuclear Medicine, 36*(7), 1238–1248.

Minoshima, S., Giordani, B., Berent, S., Frey, K. A., Foster, N. L., & Kuhl, D. E. (1997). Metabolic reduction in the posterior cingulate cortex in very early Alzheimer's disease. *Annals of Neurology, 42*(1), 85–94.

Minoshima, S., Foster, N. L., Sima, A. A., Frey, K. A., Albin, R. L., & Kuhl, D. E. (2001). Alzheimer's disease versus dementia with Lewy bodies: cerebral metabolic distinction with autopsy confirmation. *Annals of Neurology, 50*(3), 358–365.

Morbelli, S., Drzezga, A., Perneczky, R., Frisoni, G. B., Caroli, A., van Berckel, B. N., et al. (2012). Resting metabolic connectivity in prodromal Alzheimer's disease. A European Alzheimer Disease Consortium (EADC) project. *Neurobiology of Aging, 33*(11), 2533–2550.

Mori, T., Ikeda, M., Fukuhara, R., Nestor, P. J., & Tanabe, H. (2006). Correlation of visual hallucinations with occipital rCBF changes by donepezil in DLB. *Neurology, 66*(6), 935–937.

Mosconi, L., Tsui, W. H., Herholz, K., Pupi, A., Drzezga, A., Lucignani, G., et al. (2008). Multicenter standardized 18F-FDG PET diagnosis of mild cognitive impairment, Alzheimer's disease, and other dementias. *Journal of Nuclear Medicine, 49*(3), 390–398.

Neary, D., Snowden, J. S., Gustafson, L., Passant, U., Stuss, D., Black, S., et al. (1998). Frontotemporal lobar degeneration: a consensus on clinical diagnostic criteria. *Neurology, 51*, 1546–1554.

Patterson, J. C., Lilien, D. L., Takalkar, A., & Pinkston, J. B. (2011). Early detection of brain pathology suggestive of early AD using objective evaluation of FDG-PET scans. *International Journal of Alzheimer's Disease*. doi:10.4061/2011/946590.

Perani, D. (2008). Functional neuroimaging of cognition. In: M. J. Aminoff, F. Boller, & D. F. Swaab (Eds.), *Handbook of Clinical Neurology* (pp.61–111). Elsevier.

Prince, M., Bryce, R., & Ferr, C. (2011). The benefits of early diagnosis and intervention. In: Alzheimer's Disease International World Alzheimer Report 2011. Institute of Psychiatry. King's College London. Alzheimer's Disease International.

Rascovsky, K., Hodges, J. R., Knopman, D., Mendez, M. F., Kramer, J. H., Neuhaus, J., et al. (2011). Sensitivity of revised diagnostic criteria for the behavioural variant of frontotemporal dementia. *Brain, 134*(Pt9), 2456–2477.

Ridgway, G., Omar, R., Ourselin, S., Hill, D., Warren, J., & Fox, N. (2009). Issues with threshold masking in voxel-based morphometry of atrophied brains. *NeuroImage, 44*(1), 99–111.

Rorden, C., Bonilha, L., Fridriksson, J., Bender, B., & Karnath, H. O. (2012). Age-specific CT and MRI templates for spatial normalization. *NeuroImage, 61*(4), 957–965.

Salmon, E., Garraux, G., Delbeuck, X., Collette, F., Kalbe, E., Zuendorf, G., et al. (2003). Predominant ventromedial frontopolar metabolic impairment in frontotemporal dementia. *NeuroImage, 20*(1), 435–440.

Salmon, E., Kerrouche, N., Perani, D., Lekeu, F., Holthoff, V., Beuthien-Baumann, B., et al. (2009). On the multivariate nature of brain metabolic impairment in Alzheimer's disease. *Neurobiology of Aging, 30*(2), 186–197.

Sestini, S., Castagnoli, A., & Mansi, L. (2010). The new FDG brain revolution: the neurovascular unit and the default network. *European Journal of Nuclear Medicine and Molecular Imaging, 37*(5), 913–916.

Signorini, M., Paulesu, E., Friston, K., Perani, D., Colleluori, A., Lucignani, G., et al. (1999). Rapid assessment of regional cerebral metabolic abnormalities in single subjects with quantitative and nonquantitative [18F]FDG PET: a clinical validation of statistical parametric mapping. *NeuroImage, 9*(1), 63–80.

Spence, J. S., Carmack, P. S., Gunst, R. F., Schucany, W. R., Woodward, W. A., & Haley, R. W. (2006). Using a white matter reference to remove the dependency of global signal on experimental conditions in SPECT analyses. *NeuroImage, 32*(1), 49–53.

Sperling, R. A., Aisen, P. S., Beckett, L. A., Bennett, D. A., Craft, S., Fagan, A. M., et al. (2011). Towards defining the preclinical stages of Alzheimer's disease: recommendations from the National Institute on Aging-Alzheimer's Association workgroups on diagnostic guidelines for Alzheimer's disease. *Alzheimer's & Dementia, 7*(3), 280–292.

Teipel, S. J., Sabri, O., Grothe, M., Barthel, H., Prvulovic, D., Buerger, K., et al. (2013). Perspectives for multimodal neurochemical and imaging biomarkers in Alzheimer's disease. *Journal of Alzheimer's Disease, 33*(S1), S329–S347.

Teune, L. K., Bartels, A. L., de Jong, B. M., Willemsen, A. T., Eshuis, S. A., de Vries, J. J., et al. (2010). Typical cerebral metabolic patterns in neurodegenerative brain diseases. *Movement Disorders, 25*(14), 2395–2404.

Tzourio-Mazoyer, N., Landeau, B., Papathanassiou, D., Crivello, F., Etard, O., Delcroix, N., et al. (2002). Automated anatomical labeling of activations in SPM using a macroscopic anatomical parcellation of the MNI MRI single-subject brain. *NeuroImage, 15*(1), 273–289.

Wenzel, F., Young, S., Wilke, F., Apostolova, I., Arlt, S., Jahn, H., et al. (2010). B-spline-based stereotactical normalization of brain FDG PET scans in suspected neurodegenerative disease: impact on voxel-based statistical single-subject analysis. *NeuroImage, 50*(3), 994–1003.

Winblad, B., Palmer, K., Kivipelto, M., Jelic, V., Fratiglioni, L., Wahlund, L. O., et al. (2004). Mild cognitive impairment-beyond controversies, towards a consensus: report of the International Working Group on Mild Cognitive Impairment. *Journal of Internal Medicine, 256*(3), 240–246.

Yakushev, I., Hammers, A., Fellgiebel, A., Schmidtmann, I., Scheurich, A., Buchholz, H. G., et al. (2009). SPM-based count normalization provides excellent discrimination of mild Alzheimer's disease and amnesic mild cognitive impairment from healthy aging. *NeuroImage, 44*(1), 43–50.